TOWARDS ESTABLISHING A DESIGN RESISTANCE FOR HOLLOW SECTION JOINTS

MARTIN KOŽICH[1], PETR JEHLIČKA[1], FRANTIŠEK WALD[1]*,

XIAO-DING BU[2], JEFFREY A. PACKER[2], JAROMÍR KABELÁČ[3]

[1]*Department of Steel & Timber Structures, Czech Technical University in Prague, 16629 Praha, Czech Republic*
E-mail: martin.kozich@fsv.cvut.cz; petr.jehlicka@fsv.cvut.cz; frantisek.wald@fsv.cvut.cz
[2]*Department of Civil & Mineral Engineering, University of Toronto, Ontario M5S 1A4, Canada*
E-mail: deanx.bu@mail.utoronto.ca; jeffrey.packer@utoronto.ca
[3]*Department of Steel & Timber Structures, Brno University of Technology, 601 90 Brno, Czech Republic*
E-mail: kabelac.m@fce.vutbr.cz

A number of design guides and standards, with considerable international consensus, now exist for the design of welded hollow section joints in onshore and offshore construction. These, however, typically cover relatively standardized joint types, geometries and loading cases. In the event of unusual joints, it is now common for finite element (FE) modelling to be performed, but specific guidance needs to be provided on acceptable FE modelling procedures and the interpretation of the output, in order for a suitable joint design resistance to be determined. Towards this objective, this paper describes appropriate FE modelling and ultimate limit states that can be used; in particular, a 5 % ultimate strain limit state. Application of these ultimate limit states is demonstrated using validated FE models for RHS-to-RHS (rectangular hollow section) X-joints and branch plate-to-CHS (circular hollow section) joints, with branches loaded in axial tension and compression.

Keywords: Hollow sections, joints, design resistance, finite element analysis

1 Introduction

CIDECT Design Guides (DG) 1 and 3 (Wardenier et al. 2008, Packer et al. 2009), EN 1993-1-8 (CEN 2005), prEN 1993-1-8:2019 (CEN 2019), ISO 14346:2013 (ISO 2013) and AISC 360-16 (AISC 2016) all give prescriptive formulae for the ultimate design resistance of numerous hollow section joints. Most contemporary design recommendations (including CIDECT DG1, CIDECT DG3, ISO 14346:2013 and prEN 1993-1-8:2019) are based on a joint resistance (represented by the force in the branch) governed by two ultimate limits. These are: a) a peak or maximum ultimate load; and b) a load corresponding to a deformation limit of 3% b_0 or 3% d_0, where b_0 corresponds to the width of an RHS chord member and d_0 corresponds to the diameter of a CHS chord member. These deformations represent indentations, inwards or outwards, of the chord connecting surface. Importantly, the deformation limit b) is only applied if this deformation is reached prior to the joint peak load. This deformation limit was contrived by IIW in the 1990s as a means of limiting

Proceedings of the 17th International Symposium on Tubular Structures.
Editors: X.D. Qian and Y.S. Choo

Published by Research Publishing, Singapore.
ISBN: 978-981-11-0745-0; doi:10.3850/978-981-11-0745-0_093-cd

deformations at both the ultimate and service load levels in flexible joints, and it has been frequently shown to correlate reasonably well with chord-face yield-line mechanism loads in RHS joints. These two ultimate limits can be applied in research on hollow section joints using laboratory experiments or finite element (FE) analysis. Two types of FE analysis should be recognized as different from design point of view and treated differently: these are numerical experiments and numerical design calculations. With the latter, material non-linearity and large deformation behaviour can be incorporated in the FE models but, for general loading conditions, a fracture criterion needs to be included to handle tensile stresses. Different fracture criteria have been advocated, many of which are research-specific and pragmatically tailored to unique laboratory experiments. The concept of performing laboratory tests to validate a FE fracture criterion for a hollow section joint is impractical for a designer; this paper thus explores an alternative ultimate limit criterion using a limiting strain.

The notion of an ultimate strain limit for FE design is described in Annex C of EN 1993-1-5:2006 (CEN 2006) and by Wald et al. (2017), with a maximum principal strain of 5 % being advocated for the limit. It is well-known that the surface strain in a welded hollow section joint increases very rapidly as the measuring point becomes close to the toe of a weld. In fatigue design, CIDECT DG 8 (Zhao et al. 2000) uses a distance of 0.4 t_0 (but ≥ 4 mm) from the weld toe as a point of rapid strain increase, hence hot-spot strain (and stress) extrapolation methods use this as the nearest point of strain measurement, in both laboratory experiments and FE analyses. In the following application to RHS joints, stand-off distances of 0.25 t_0, 0.4 t_0, 0.5 t_0 and 1.0 t_0 from the weld toe are used for the strain measuring location. The maximum principal strain, either tensile or compressive, is then monitored at all positions around the hollow section joint at, or greater than, this stand-off distance.

2 Application to RHS-to-RHS joints

2.1 *Model and validation*

Sixteen laboratory experiments performed by Fan and Packer (2017) on T-shaped RHS-to-RHS joints have been used to validate the FE models. FE modelling was performed with commercial software ANSYS v18.1, using 3D eight-noded solid elements (SOLID185). Actual measured dimensions were used for the geometry and non-linear material properties were assigned based on tensile coupon tests. To match the experiments, the modelled joints were loaded with axial compression in the branch, while the opposite side of the chord was supported by a rigid contact surface. The FE model and validation of a representative joint are presented in Fig. 1. Since the joint has two planes of symmetry, only a quarter of the joint is modelled. A comprehensive mesh optimization study was also performed to validate the FE model.

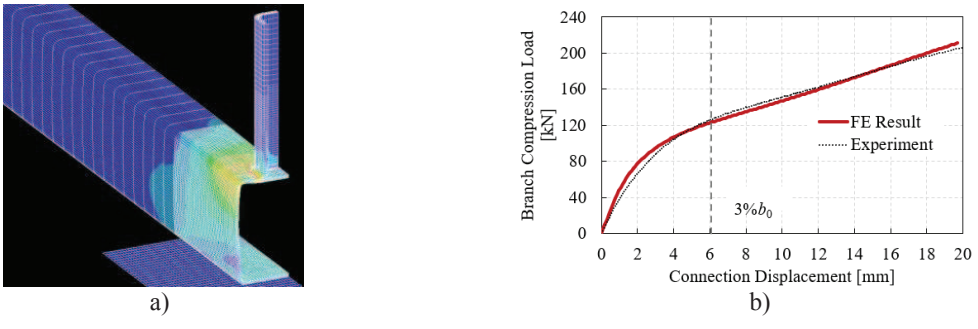

Figure 1. FE model validation, for a representative joint $\beta = 0.5$: a) typical FE meshing and stress distribution; b) corresponding branch load-displacement for FE model and experiment

2.2 *Sensitivity study*

After validation of the T-shaped model, X-shaped joint models were created with one more plane of symmetry. Four square-member RHS-to-RHS 90° X-joints were analysed with both axial tension and compression branch loading. The corresponding load-displacement curves and the 3 % ultimate deformation limits are shown in Figs. 2-5. The chord member used for all joints was RHS200x200x8, while the branch member depends on the branch-to-chord width ratio, β. Thick branches were used to ensure that the branches were non-critical, corner geometries were typical of cold-formed RHS, and mechanical properties replicated those in the FE validation models.

In all joints, the maximum principal strain was measured at distances of 0.25 t_0, 0.4 t_0, 0.5 t_0, and 1.0 t_0 from the weld toe. The distance of 0.25 t_0 corresponds to the size of the chord element, since models used four elements through the chord thickness. The distance of 0.4 t_0 is central to the CIDECT strain extrapolation method for fatigue design. At these particular distances, multiple nodes were monitored to ensure that the maximum-strain node was detected. Also, nodes on both the outer and inner surfaces of the chord were tracked at the stand-off distance. During the analyses, the strain in the branch was also measured at the same distance from the weld toe, to ensure that the branch did not reach 5% maximum strain prior to the chord.

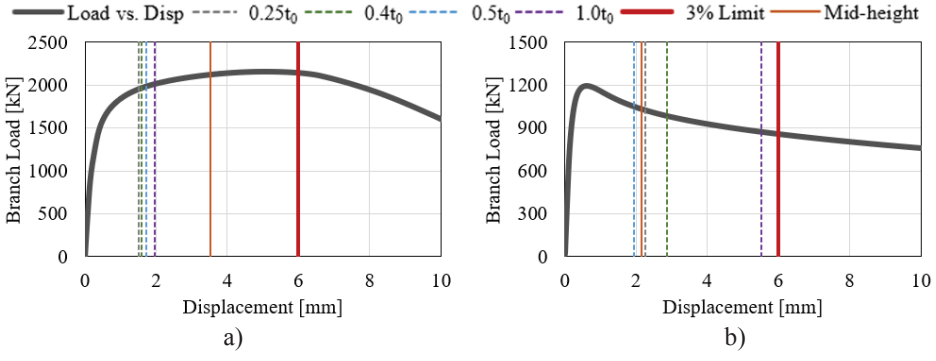

Figure 2. RHS-to-RHS 90° X-connection, with 200x200x8 chord, β = 1.0, loaded: a) in branch tension; b) in branch compression

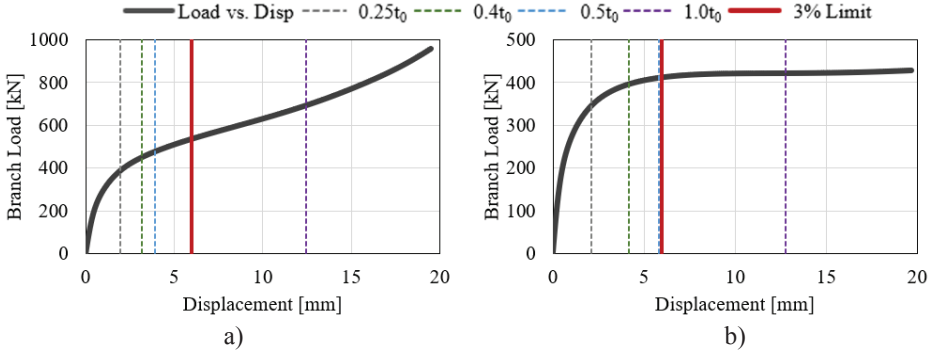

Figure 3. RHS-to-RHS 90° X-connection, with 200x200x8 chord, β = 0.75, loaded: a) in branch tension; b) in branch compression

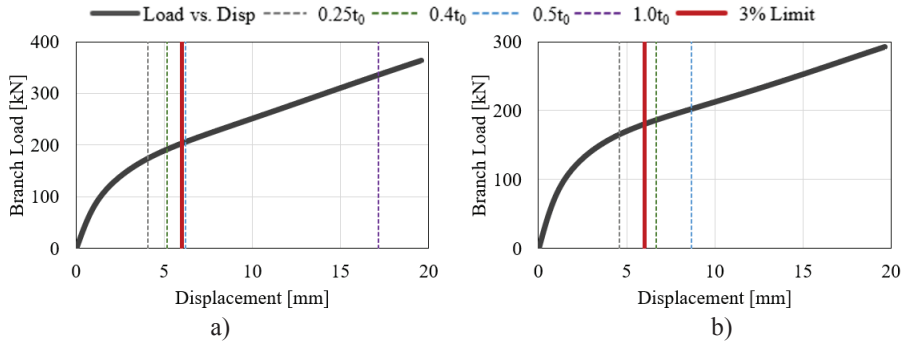

Figure 4. RHS-to-RHS 90° X-connection, with 200 x 200 x 8 chord, $\beta = 0.5$, loaded: a) in branch tension; b) in branch compression

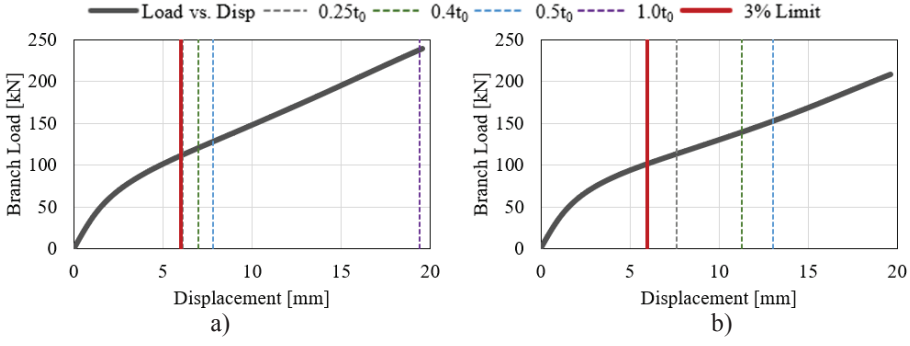

Figure 5. RHS-to-RHS 90° X-connection, with 200x200x8 chord, $\beta = 0.25$, loaded: a) in branch tension; b) in branch compression

The displacements corresponding to the governing 5 % strain are illustrated in each Figure by dashed vertical lines. In Fig. 2, the maximum strain at chord mid-height was also measured, as it governs the compressive strength for matched-width joints, see Fig. 2b. For $\beta = 1.0$ in branch tension, see Fig. 2a, all measuring distances provide a conservative limit on the predicted ultimate load; for $\beta = 1.0$ in branch compression, see Fig. 2b, the mid-height-strain load is close to the peak load but monitoring the peak load in conjunction with the 5 % strain load serves as a check in buckling cases such as this. For $\beta = 0.75$, in both branch tension and compression, Fig. 3, the joint is somewhat flexible, and the 5 % strain load at 0.4 t_0 or 0.5 t_0 serves as a conservative but close predictor of the 3% ultimate deformation limit. For $\beta = 0.50$, in both branch tension and compression, Fig. 4, the joint is moderately flexible, and the 5 % strain load at 0.4 t_0 or 0.5 t_0 serves as a good predictor of the 3 % ultimate deformation limit. For $\beta = 0.25$, the joint is very flexible and the 5 % strain load at 0.4 t_0 or 0.5 t_0 is again a good predictor of the 3 % ultimate deformation limit in branch tension, Fig. 5a; in branch compression, Fig. 5b, the correlation is less close but, for such low-β joints, there is a huge reserve of load capacity beyond the 3 % deformation limit.

The results for each of the eight joints are summarized in Table 1, where the 5 % strain resistance and the 3 % deformation limit strength, are listed for each measuring distance. It is observed that the results at a stand-off distance of 0.4 t_0 or 0.5 t_0 generally match the 3 % deformation limit resistance better than others, hence favouring these measurement distances.

Table 1. Strengths predicted using 5 % maximum principal strain limit for RHS-to-RHS connections

β	Load	Strength (kN), and Strength / 3% Deformation limit strength								3 % Deformation limit strength
		0.25 t_0		0.4 t_0		0.5 t_0		1.0 t_0		
1.0	T	1952	91%	1963	91%	1983	92%	2010	93%	2154
	C	1193	-	1193	-	1193	-	1193	-	1193*
0.75	T	392	72%	449	82%	481	88%	720	132%	546
	C	344	85%	389	96%	405	100%	413	102%	406
0.5	T	177	86%	194	95%	207	101%	339	165%	205
	C	167	92%	187	103%	203	112%	- **		181
0.25	T	107	100%	116	108%	123	115%	232	217%	107
	C	108	111%	133	137%	146	151%	- **		97

*Peak load governs

**Results beyond the range of analysis

3 Application to Branch Plate-to-CHS joints

3.1 *Model, validation and verification*

The model, prepared with the FE program ABAQUS v6.14, was built from eight-noded brick elements with reduced integration (C3D8R). The calculation uses materially and geometrically nonlinear analysis with a true stress-true strain material diagram. The mesh size was 3 mm, reached by sensitivity study with a 4.7 % error. The model was validated and verified by experiments and numerical simulations of T- and X-shaped plate-to-CHS specimens prepared at University of Toronto (UofT) by Voth and Packer (2010). The geometry of three tested CHS specimens and their material properties are summarized in Table 2, where d_0 is the chord diameter, t_0 is the chord web thickness, b_1 is the connected plate width, t_1 is the connected plate thickness and l_0 is the chord length. The geometry is described by ratios $\beta = b_1 / d_0$ and $2\gamma = d_0 / t_0$.

The specimen CX90EC-D1-13 is an X-joint with transversely welded plates loaded in axial compression, CB90EA is a T-joint with a transversely welded plate loaded in axial tension, and CX0ET-D1-69 is an X-joint with longitudinally welded plates loaded in axial tension. Fig. 6a shows a typical distribution of principal strain in the weld toe region. The force - deformation curves in Fig. 6b,c,d show deformation of the chord surface by the force acting in the branch member. The solid lines represent experimental results, dotted UofT numerical results and the dashed ones the results of a CTU numerical simulation. The models were checked for applied load at 6 mm of chord deformation, which is close to the design limit of 3 % d_0 deformation. The correlation between FE and experimental branch loads at this displacement shows reasonable accuracy, with differences up to 4 %, see Table 3.

Table 2. The geometry and material properties of CHS specimens selected for validation of CTU model

Specimen	d_0 (mm)	t_0 (mm)	b_1 (mm)	t_1 (mm)	l_0 (mm)	β or η	2γ
CX90EC-D1-13	219.1	11.10	131.5	19.05	2236.9	0.60	19.74
CB90EA	219.1	4.49	100.3	18.99	557.8	0.46	48.93
CX0ET-D1-69	219.1	6.35	657.3	19.05	2875.2	3.0	34.50

Cross section	Modulus E (GPa)	Yield strength f_y (MPa)	Strength f_u (MPa)
CHS	211	389	527
Plates	210	326	505

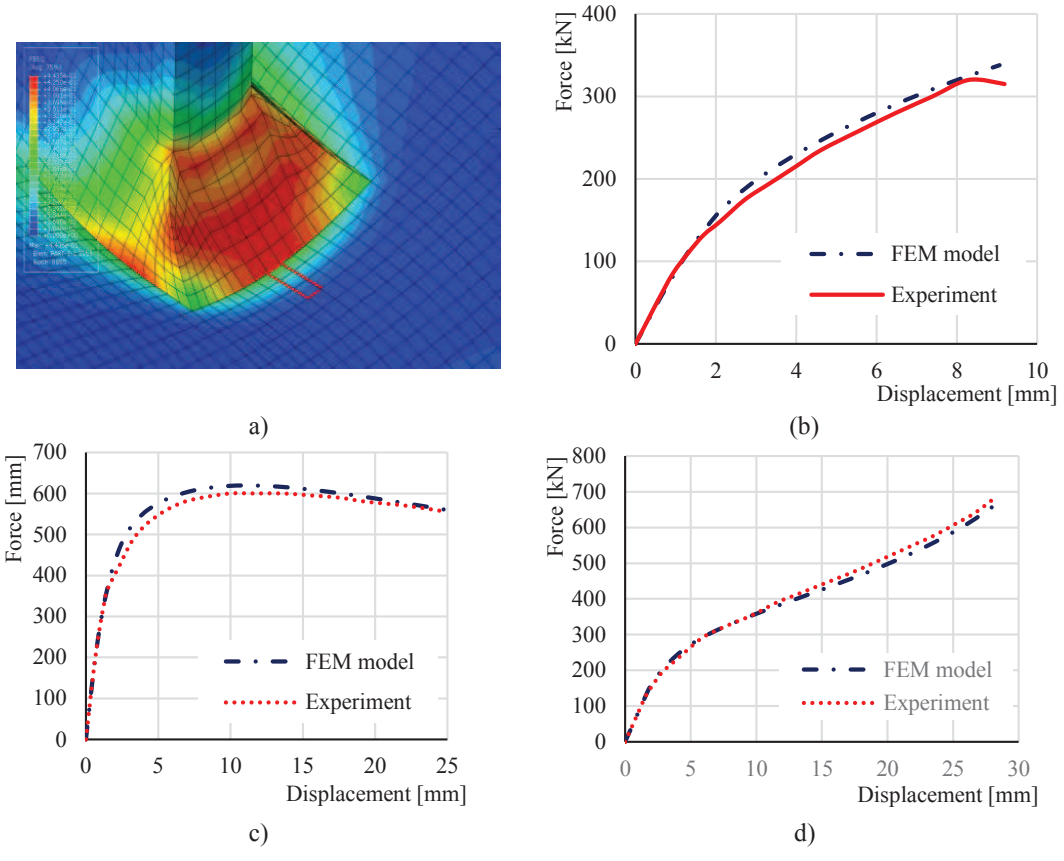

Figure 6. a) Principal strain in the entire strip 0.5 t_0 around the connected branch weld in the direction of the main tensile strain, b) validation of CVUT FE model on experiment CB90EA, T-joint in tension, c) verification of CVUT FE model on CX90EC-D1-13, X-joint in compression, and d) verification of CVUT FE model on CX0ET-D1-69, X-joint in tension

Table 3. Prediction of joint behaviour at 6 mm deformation of upper surface of chord

Specimen		CTU FEM model	Experiment/UofT FEM model	Ratio
		Force at 6 mm def.	Force at 6 mm def.	
CB90EA	Physical	279.8 kN	268.5 kN	1.04
CX90EC-D1-13	Numerical	591.3 kN	566.6 kN	1.04
CX0ET-D1-69	Numerical	294.0 kN	294.3 kN	1.00

3.2 *Sensitivity study*

For different joint types and different loading conditions there are, from the force - deformation diagram point of view, four types of curve shapes. Shape A - 5 % limit of strain in the strip is reached while the load-bearing capacity of the joint increases on a convex curve to a peak load, see Fig. 7a. Shape B - 5 % limit of strain is reached while the load-bearing capacity of the joint increases on a convex curve till the limit of the test set up is reached, see Fig. 7b. Shape C - a joint local maximum is reached after the 5 % limit of maximum principal strain in the strip, see Figure 3a. Shape D – a joint peak load is reached before the 5 % limit of strain, see Fig. 2b.

Resistances, predicted by the 5 % strain limit and the 3 % d_0 deformation limit, are compared on FE simulations (previously validated on experiments) for three types of these force -

deformation diagrams in Fig. 7 and summarized in Table 4. The biggest difference, see Fig. 7b, is observed in the case where the load-bearing capacity of the joint increases on a convex curve, where a T-joint with a transverse plate is subject to a branch tension load and the joint has limited deformation capacity ($\beta = 0.5$). Nevertheless, the difference between the 5% strain limit and the 3% d_0 deformation limit is acceptable, with the 5% strain limit being more conservative.

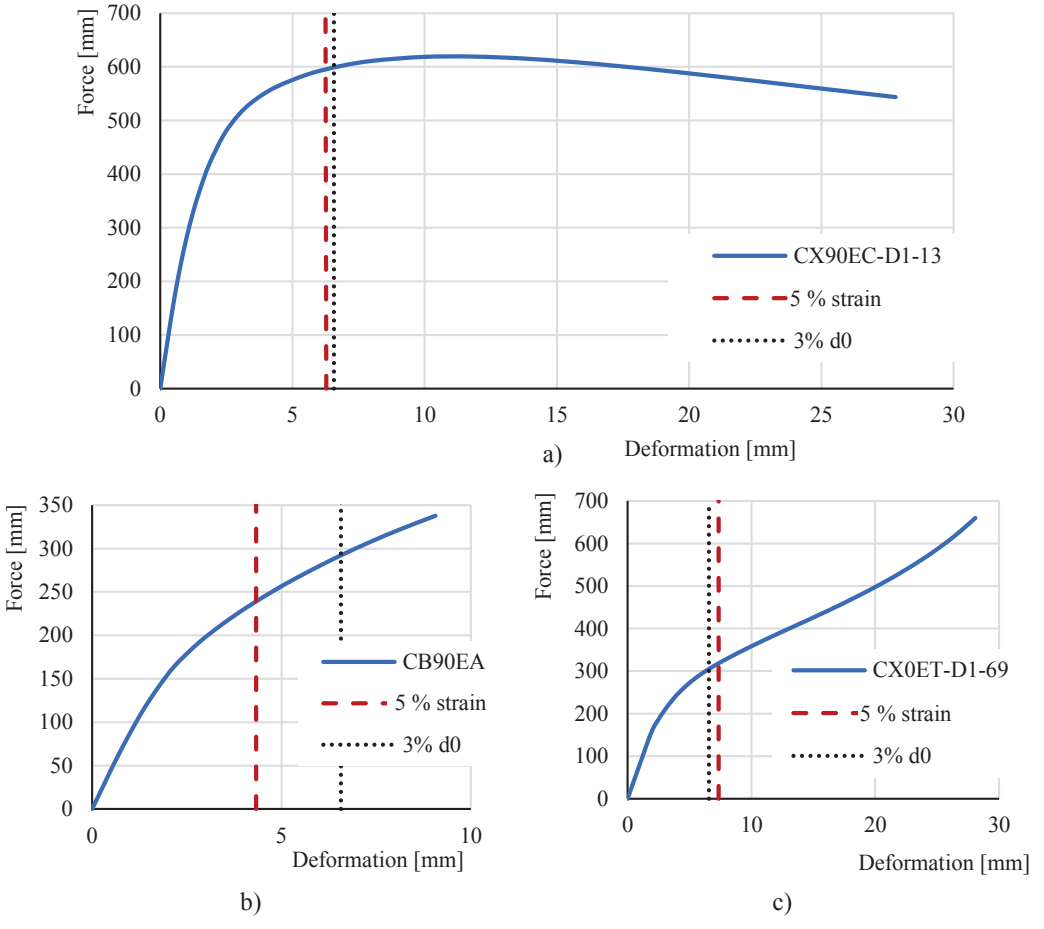

Figure 7. Comparison of resistance predicted as 5 % strain limit and 3 % d_0 deformation limit for specimen a) CX90EC-D1-13, X-joint in compression, b) CB90EA, T-joint in tension, and c) CX0ET-D1-69, X-joint in tension

Table 4. Difference in resistance predicted as 5 % strain limit and 3 % d_0 deformation limit

Specimen	5 % strain limit	3 % d_0 deformation limit	Comparison
CB90EA	238.9 kN	292.2 kN	0.81
CX90EC-D1-13	594.4 kN	598.4 kN	0.99
CX0ET-D1-69	319.0 kN	304.8 kN	1.04

4 Conclusion

Based on numerical studies and literature observations it is recommended that, for the design of hollow section welded joints using finite element analysis, applying either solid or shell elements, the joint design resistance should be evaluated as:

(i) the load corresponding to a 5 % maximum principal strain, in the entire strip at a distance of 0.5 t_0 from the weld toe around the connected branch, where t_0 is the thickness of the chord,
(ii) the peak load, if it occurs at a maximum principal strain < 5 %.

Acknowledgments

Financial support for this project was provided by the Natural Sciences and Engineering Research Council of Canada (NSERC) and the Technology Agency of the Czech Republic (TAČR).

References

AISC, *ANSI/AISC 360-16, Specification for Structural Steel Buildings,* American Institute of Steel Construction, Chicago, 2016.

CEN, EN 1993-1-5, Eurocode 3: Design of Steel Structures – Part 1-5: Plated structural elements, European Committee for Standardization, Brussels, 2006.

CEN, EN 1993-1-8, Eurocode 3: Design of Steel Structures – Part 1-8: Design of Joints, European Committee for Standardization, Brussels, 2005.

CEN, prEN 1993-1-8, Eurocode 3: Design of Steel Structures – Part 1-8: Design of Joints, European Committee for Standardization, Brussels, 2019.

Fan, Y. and Packer, J. A., RHS-to-RHS Axially Loaded X-Connections Near an Open Chord End, *Can. J. Civ. Eng*. 44, 881-892, 2017.

ISO, ISO 14346:2013, Static Design Procedure for Welded Hollow-section Joints - Recommendations, International Organization for Standardization, Switzerland, 2013.

Packer, J.A., Wardenier, J., Zhao, X.L., van der Vegte, G.J. and Kurobane, Y., CIDECT Design Guide No.3, Design Guide for Rectangular Hollow Section (RHS) Joints under Predominantly Static Loading, 2nd Ed., CIDECT, Geneva, 2009.

Voth, A.P., Packer, J. A., *Branch plate-to-circular hollow structural section connections*, CIDECT Final Report 5BS-3/10, University of Toronto, 2010.

Wald, F., Sabatka, L., Bajer, M., Barnat, J., Godrich, L., Holomek, J., Jehlicka, P., Kabelac, J., Kocka, M., Kolaja, D., Kral, P., Kurikova, M. and Vild, M., *Benchmark cases for advanced design of structural steel connections*, 2nd extended edition, Czech Technical University in Prague, 2017.

Wardenier, J., Kurobane, Y., Packer, J.A., Dutta, D. and Yeomans, N., CIDECT Design Guide No.1, Design Guide for Circular Hollow Section (CHS) Joints under Predominantly Static Loading, 2nd Ed., CIDECT, Geneva, 2008.

Zhao, X.-L., Herion, S., Packer, J.A., Puthli, R.S., Sedlacek, G., Wardenier, J., Weynand, K., van Wingerde, A. M. and Yeomans, N.F., *CIDECT Design Guide No.8, Design Guide for Circular and Rectangular Hollow Section Welded Joints under Fatigue Loading*, CIDECT, Geneva, 2000.